TRR
JOURNAL OF THE TRANSPORTATION RESEARCH BOARD

Article

Transportation Research Record
1–10

DOI: 10.1177/0361198118759005
journals.sagepub.com/home/trr
SAGE

Identification and Calculation of Horizontal Curves for Low-Volume Roadways Using Smartphone Sensors

Jonathan S. Wood[1] and Shaohu Zhang[2]

Abstract

Horizontal curves are a contributing factor to the number of observed roadway crashes. Identifying locations and geometric characteristics of horizontal curves plays a crucial role in crash prediction and prevention. However, most states in the USA face a challenge in maintaining detailed and high-quality roadway inventory databases for low-volume rural roads due to the labor-intensive and time-consuming nature of collecting and maintaining the data. This paper proposes a low-cost mobile road inventory system for two-lane horizontal curves based on off-the-shelf smartphones. The proposed system is capable of accurately detecting horizontal curves by exploiting a K-means machine learning technique. Butterworth low-pass filtering is applied to reduce sensor noise. Extended Kalman filtering is adopted to improve the GPS accuracy. Chord method-based radius computation and superelevation estimation are introduced to achieve accurate and robust results despite the low-frequency GPS and noisy sensor signals obtained from smartphones. This study implements this method using an Android-based smartphone and tests 21 horizontal curves in South Dakota. The results demonstrate that the proposed system achieves high curve identification accuracy as well as high accuracy for calculating curve radius and superelevation.

Two-lane roadways comprise the predominant road type in most countries. There are more than three million miles of two-lane highways in the USA, 90% of which carry traffic volumes of fewer than 2000 vehicles per day (*1*). According to the Fatality Analysis Reporting System (FARS), in 2014 66.4% (29,796 out of 44,858) fatal crashes occurred on two-lane roadways. Also, 20.1% (7656 out of 38,046) of single- and two-vehicle fatal crashes occurred along horizontal curves (*2*). Knowledge of locations and geometric characteristics of the roadway curves on low-volume roads play a crucial role in crash prediction and prevention. Although some states collect and store roadway curve data, including curve-related information (i.e., degree of curvature) on US and state highways, it is typically incomplete curve information (e.g., lacking information such as superelevation) (*3*). There is high demand for this information on rural roads for use in engineering design, safety management, and determining appropriate advisory speeds. This is a particularly important issue given that the Federal Highway Administration (FHWA) has mandated that all highway transportation agencies (state, local, and so forth) survey all roadway horizontal curves by December 31, 2019 (*4*).

Mobile asset data collection vehicles equipped with sensors such as LiDAR (light detection and ranging), GPS (Global Positioning Signal), and inertial measurement units (IMU) can provide transportation agencies with location information and roadway design elements, including horizontal curve properties. However, users need to be familiarized with detailed and tedious device procedures as well as post-data-collection processes. In addition, the cost for a survey vehicle with this equipment can be prohibitive for many agencies and researchers. Smartphones that integrate GPS, IMU, and advanced computing technologies have become more accessible owing to affordable price, product innovation, and people's desire to be connected. As more people own these devices, there are greater opportunities for data acquisition in intelligent transportation systems, which turns them into low-cost, real-time mobile sensor platforms.

This study provides a novel approach to automatically identify and measure horizontal curves using smartphone sensors. Smartphones have low-cost sensors chips. These low-cost sensors allow smartphones to have GPS and accelerometer technology without causing a significant increase in the cost of purchasing smartphones. However, the low cost is associated with a reduction in accuracy compared to more expensive sensors. Thus, when using these sensors, it is critical to utilize methods that improve the sensors' accuracy. This requires a system that (1) accounts for and reduces

[1]Department of Civil and Environmental Engineering, South Dakota State University, Brookings, SD
[2]Department of Computer Science, North Carolina State University, Raleigh, NC

Corresponding Author:
Address correspondence to Jonathan S. Wood: woohon@gmail.com

sensor (e.g., gyro and accelerometer) measurement errors and outliers; (2) reduces the location error caused by the weak GPS signals or GPS outage; and (3) provides a cost-effective real-time mobile system that detects horizontal curves and calculates their parameters accurately and reliably (e.g., radius and superelevation).

Literature Review

Many agencies and researchers have shown an interest in the extraction and identification of horizontal curves. Common curve identification techniques employed involve geographic information systems (GIS) based tools, satellite imagery processing, and mobile asset data collection. GIS-based tools (*3,5,6*) can extract and identify horizontal curves from GIS roadway maps in large-scale networks. However, the GIS-based techniques require high-quality GIS data to reduce identification errors from transverse measurement errors and low vertex resolution of GIS roadway centerlines. In addition, it is not possible to evaluate the superelevation of horizontal curves based on standard GIS data and tools because of lack of data or data resolution that is not fine enough. Image processing using high-resolution satellite imagery (*7–10*) can retrieve geometric characteristics of some typical curves; the drawbacks are that the accuracy greatly relies on image resolution and that it requires processing of many high-resolution images. Thus, these methods incur high computational costs. Also, none of these methods can extract information on the superelevation for horizontal curves.

A survey vehicle equipped with a GPS receiver, inertial system, and other sensors (including LiDAR) is another way to collect data and construct roadway asset inventories. The collected raw GPS data are postprocessed to extract horizontal curve components. Harkey et al. (*11*) discussed how the azimuth data obtained from the instrumented vehicle can be a useful tool for identifying curves and tangents on the roadway. However, the data collection and the postprocessing methods need to be improved to measure the radius and length of horizontal curves accurately. Carlson et al. (*12*) identified and tested 10 techniques (i.e., basic ball bank indicator [BBI], advanced BBI, chord length, compass, field survey, GPS, lateral acceleration, plan sheet, speed advisory plate, and vehicle yaw rate) to obtain horizontal curve radii. Based on the results, the in-vehicle GPS method was recommended to record roadway alignment for field personnel. To evaluate the accuracy of horizontal alignment data from multiple commercial roadway inventories, Findley et al. (*13*) applied five different techniques (i.e., chord method, GIS method, vendor data, survey data, and design data) to obtain curve parameters. The results were compared with the vendors' data, and the authors argued that agencies should consider the limitations of each technique to collect appropriate data to meet their needs. Laser scanning technology (*14*) can provide highly accurate survey data, which can be utilized to extract horizontal and vertical alignment of a curve. However, its cost is higher than that of other approaches – it was reported that the cost per mile to obtain the required highway inventory dataset for photo/video log, satellite/aerial imagery, and GPS data logger were $72, $107, and $700, respectively, while the mobile LiDAR was $915 (*15*). In addition, users must be familiarized with operating instructions. Finally, the postprocessing of raw data from these systems is time-consuming and labor-intensive.

Most smartphones are equipped with a series of sensors, including an accelerometer, gyroscope, barometer, magnetic sensor, and GPS. This richness in sensors enables support for roadway inventory in a low-cost manner. Recently, studies have been published using smartphone sensing in vehicles. GPS-related applications are applied to position capturing (*16,17*) or to vehicle tracking (*18*). Accelerometers have been used in studies to measure potholes (*19,20*) or pavement roughness (*21,22*). Won et al. (*23*) applied the barometer sensor of a smartphone to extract unique elevation signatures of driving routes. Zhang et al. (*24*) presented a mobile system to detect horizontal curves by synthesizing smartphone sensor data to generate curve models by applying a support vector machines learning technique.

Methodology

The basic concept of the proposed system is to use the rotation rate around the *z*-axis of the gyroscope to identify when a vehicle negotiates a horizontal curve. The corrected GPS location can be applied to identify the PC (point of curvature) and PT (point of tangent) of a curve, which can then be used to calculate the curve radius. Figure 1 illustrates the coordinate relationship between the vehicle and smartphone.

The system has four main system modules: data collection, data correction, curve identification, and curve calculation, as shown in Figure 2. The system takes real-time sensor readings from the smartphone – including the GPS, accelerometer, and gyroscope readings – in the data collection module. The data correction module reduces the noise of the raw input data. The Butterworth low-pass filter is applied to smooth the acceleration rate (m/s^2) and rotation rate (rad/s). GPS and speed data are corrected by applying the extended Kalman filter (EKF) algorithm. The curved road segments can be easily detected based on the smoothed rotation rate around the *z*-axis. Once the filtered curved segment data is identified, the curve identification module implements a K-means machine learning algorithm to evaluate the segment data and then determine if it is the horizontal curve. The obtained sensor data from the curves are imported to the curve calculation module. The filtered GPS data are used to identify the PC and PT of a curve, then to calculate the radius. Superelevation is calculated using the obtained radius, speed, and acceleration rate in the lateral direction.

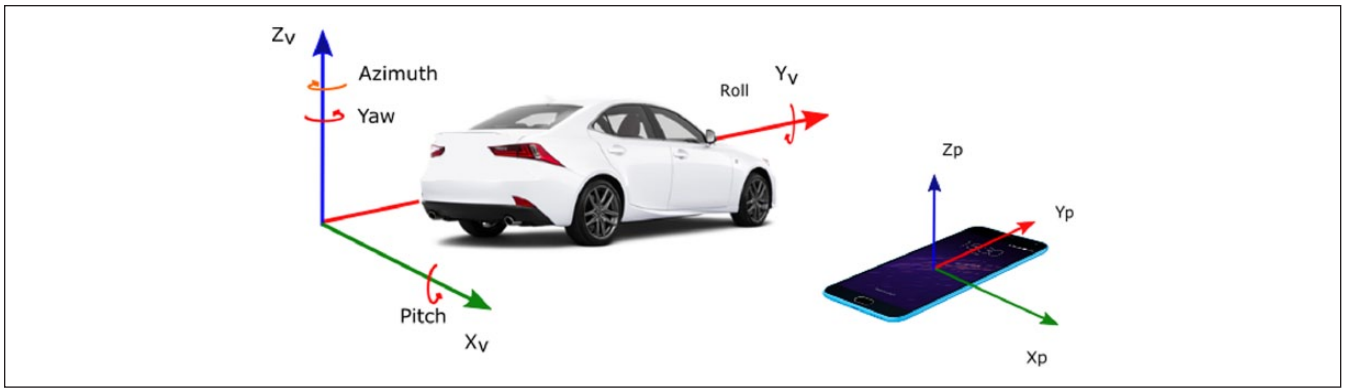

Figure 1. The coordinate systems of a smartphone and a vehicle.

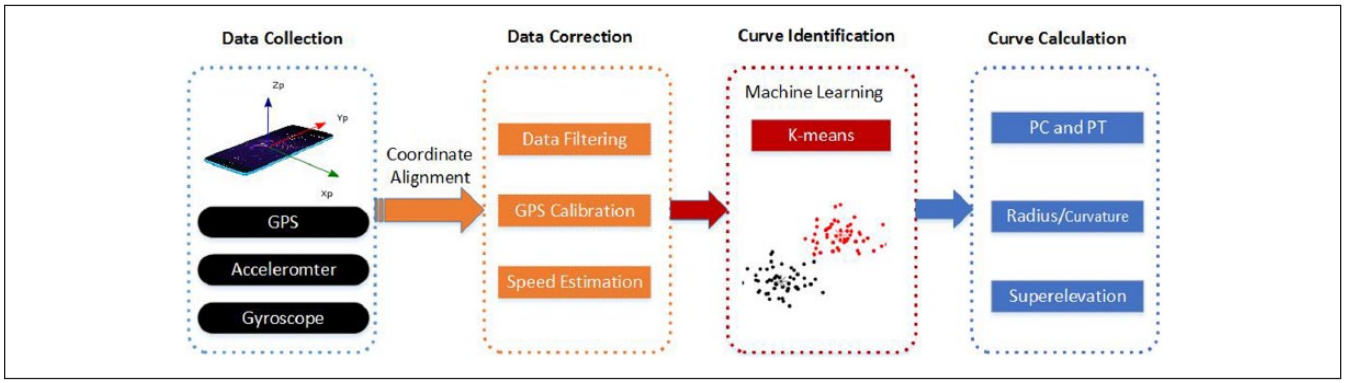

Figure 2. System architecture.

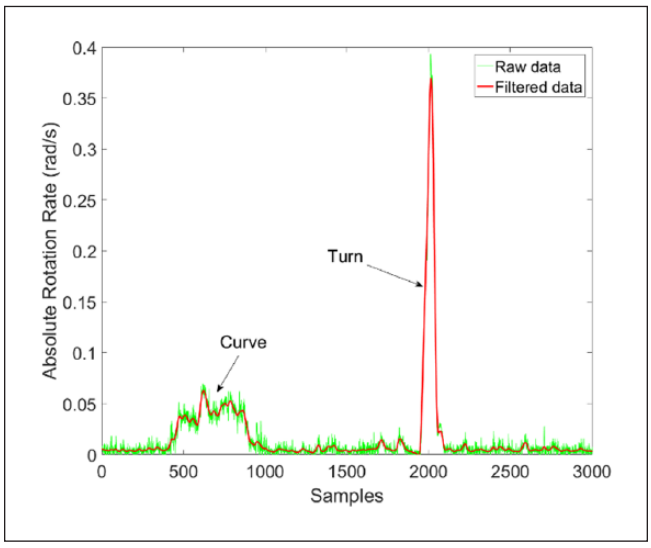

Figure 3. Variation of the angular speed around the *z*-axis.

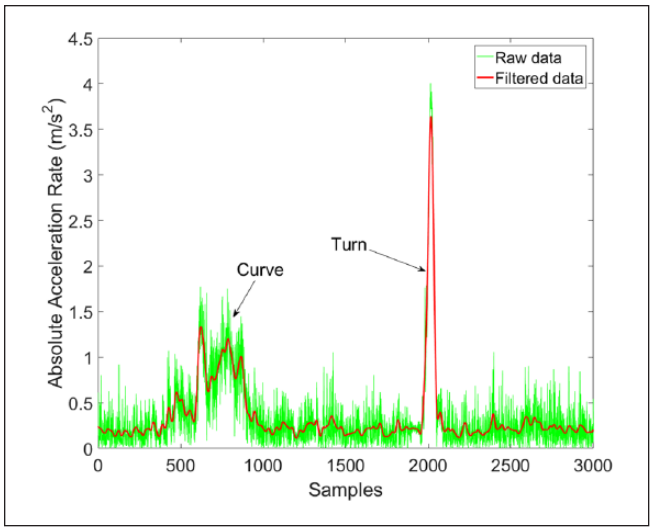

Figure 4. Variation of the acceleration rate on the *x*-axis.

Butterworth Low-Pass Filter

It is crucial to minimize measurement noise and outliers to achieve accurate curve detection and speed estimation. The Butterworth low-pass filter is well known for its effectiveness to reduce noise of high-frequency measurements *(25)*. This technique is adopted to remove the noise of raw accelerometer and gyroscope data collected using a smartphone. Figures 3 and 4 plot measurements of rotation rate around the *z*-axis and acceleration rate on the *x*-axis for a turning and a roadway

Figure 5. Raw GPS locations (red) versus smoothed GPS locations (green).

curve, respectively. It is shown that the noise is effectively removed by applying the Butterworth low-pass filter.

Extended Kalman Filtering

This system requires accurate measurement of the vehicle's GPS location and speed to derive the horizontal superelevation. The smartphone can acquire the speed reading from the embedded GPS module when the GPS signal is strong. The acceleration rate and rotation rate from IMU readings can be used to calibrate the vehicle's speed and locations when the GPS signal is weak or there is a signal outage.

The EKF is the nonlinear version of the Kalman filter, which linearizes an estimate of the current mean and covariance. The EKF is considered the de facto standard in the theory of nonlinear state estimation, navigation systems, and GPS. Assuming the process has a state vector x_k, and letting $f()$ denote the nonlinear function, the recursion equations for EKF are given as follows *(26)*:

$$x_k = f\left(x_{k-1}, u_{k-1}, w_{k-1}\right) \tag{1}$$

$$z_k = h\left(x_k, v_k\right) \tag{2}$$

where u_{k-1} is the control vector; w_{k-1} and v_k represent the process and measurement noises, which are both assumed to be zero mean multivariate Gaussian noises with covariance Q_k and R_k, respectively. The nonlinear function $h()$ relates to the state x_k to the measurement z_k.The state vector x is given in Equation 3:

$$x = \begin{Bmatrix} lat, lon, att, v_x, v_y, v_z, w_x, \\ w_y, w_z, acc_x, acc_y, acc_z \end{Bmatrix} \tag{3}$$

where v is the speed, w is the rotation rate, and acc is the acceleration rate. When the GPS signal is weak or there is an outage, the speed can be evaluated by the acceleration rate, and the GPS can be estimated by the rotation rate and speed. Figure 5 demonstrates that the GPS accuracy is improved by using the EKF.

Identification of Horizontal Curves

To distinguish between horizontal curves and lane change or turning maneuvers, this study adopted a K-means machine learning technique. K-means is one of the common "clustering" unsupervised machine learning techniques. It partitions n observations into k clusters in which each observation belongs to the cluster with the nearest mean value. Suppose a dataset D contains *n* objects in Euclidean space, which can be partitioned into k clusters *(27)*. A centroid-based partitioning technique uses the centroid of a cluster C_i to represent the *i*th cluster. The centroid can be determined by the mean of the clusters *(27)*.

The Euclidean distance $dis\left(p, c_i\right)$ measures the distance between the object point p and the centroid c_i. The sum of squared error between all objects in C_i is used to determine the centroid of cluster C_i, which can be defined as *(27)*:

$$SSE = \sum_{i=1}^{k} \sum_{p \in C_i} dis\left(p, c_i\right)^2 \tag{4}$$

where p represents any given observation, and c_i is the centroid of cluster C_i.

With K-means clustering, a threshold is selected to remove the data from the tangent road sections. It was observed that the standard deviation and mean of the rotation rate around the *z*-axis have a set of clustering features. Consequently, this study was able to use K-means clusters analyzing the rotation rate around the *z*-axis and determines whether that movement is a turn or a curve. A K-means algorithm, with K = 2, is applied to partition the training dataset into two clusters which represent curves and turns, respectively. Specifically, a centroid-based partitioning technique (*28*) was used to obtain the centroid of a cluster C_i to represent clusters. As shown in Figure 6, 50 curves and 50 turns were used to train the clustering centroids for the standard deviation and the mean of the rotation rate around the *z*-axis. To identify horizontal curve displacement, a threshold (0.01 rad/s) of the rotation rate was set to obtain the points in array *A* which represent the curved section of the vehicle's position (e.g., lane change, turns, and curve). The array *A*, representing a curved road, is considered if the Euclidean distance with the centroid of curve clustering c_i is the smallest one, based on Equation 5:

$$d = dis\left(A, c_i\right) \tag{5}$$

where d is the Euclidean distance between *A* and the *i*th centroid of the mean and standard deviation of the rotation

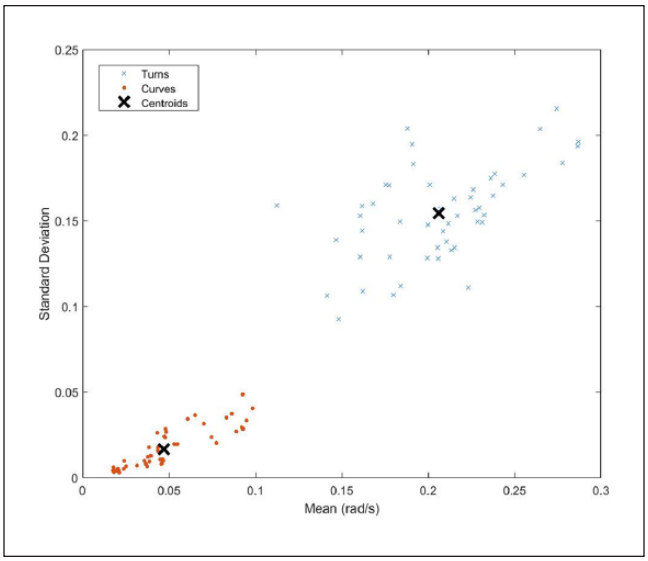

Figure 6. Cluster assignments and centroids of the rotation rate around the z-axis.

rate around the *z*-axis, and A is an array of the filtered rotation rate around the *z*-axis.

Calculation of Horizontal Curves

Chord Offset Method. A chord offset method is adopted to calculate curve radius. To improve the accuracy, three location measurements were recorded within the boundaries of PC and PT for each horizontal curve. In Figure 7, R represents the radius of the circle in feet; C is the chord length in feet; and H is the middle ordinate in feet. The radius in H and C can be derived by using:

$$\frac{C^2}{4}+\left(R-H\right)^2=R^2 \tag{6}$$

$$R=\frac{H}{2}+\frac{C^2}{8H}\pm\frac{\text{Lane width}}{2} \tag{7}$$

$$D=\frac{5729.38}{R} \tag{8}$$

The GPS frequency rate is 1 Hz in the majority of modern smartphones. Owing to the slow rate, it cannot properly capture the locations of the PC and PT for roadway horizontal curves using GPS alone. The gyroscope has a much higher output rate, which can be used to identify the locations of PC and PT. More specifically, the count of samples in rotation rate over a specified threshold when the vehicle is traversing a curved road segment is used. This calculated proportion can be used to find the location between a point on the tangent and the next point on the curved road segment.

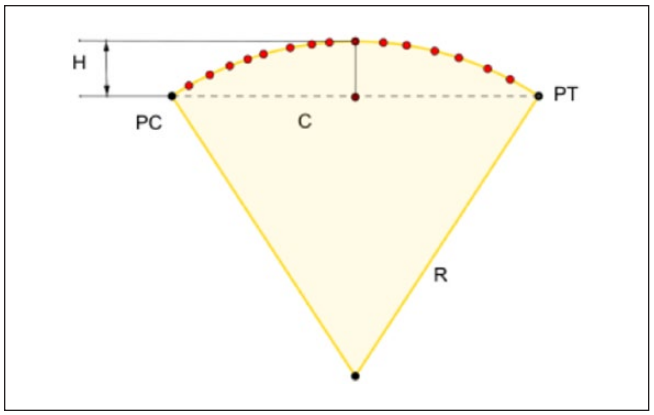

Figure 7. Chord offset method for curve radius measurement.

The chord method can be used to estimate the radius of the curve. This method can be sensitive to where middle ordinate measurements are taken. To improve the accuracy of curve radius estimates, the three neighboring GPS points around the PC and PT (within the extents of the curve) can be used to obtain nine chord lengths $\left(C\right)$ and nine middle ordinate $\left(H\right)$ measurements, respectively. Equation 9 was used to calculate the chord lengths based on the observed data. Then the calculated R_i was averaged using the weighted average method shown in Equation 10:

$$C_i=dis\left(PC_j,PT_k\right) \tag{9}$$

$$R_{avg}=\frac{\sum_{i=1}^{9}R_iH_i}{\sum_{i=1}^{9}H_i} \tag{10}$$

Superelevation Estimation. The lateral acceleration and vehicle speed measurements from the smartphone can be used to calibrate the superelevation. According to the AASHTO *Green Book* (*29*):

$$\frac{0.01e+f}{1-0.01ef}=\frac{v^2}{15R}\approx 0.01e+f \tag{11}$$

$$R=\frac{v^2}{15\left(0.01e+f\right)} \tag{12}$$

$$e=100\left(\frac{v^2}{15R}-f\right) \tag{13}$$

where e is the superelevation in percent, f is the side-friction factor (which is equivalent to X_{acc}/g, where X_{acc} is the acceleration rate on the side of the vehicle measured by the smartphone), and v is the vehicle speed in miles per hour. Thus, using the calculated radius, vehicle speed, and lateral acceleration from the smartphone sensors (to obtain an estimate of f), superelevation is estimated.

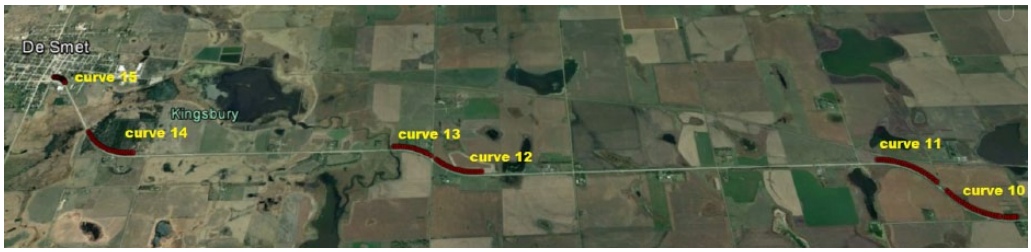

Figure 8. Test section with six identified horizontal curves.

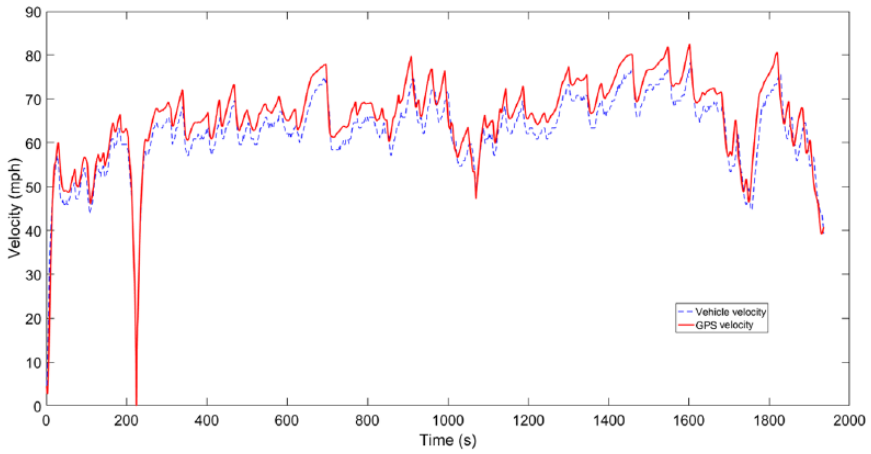

Figure 9. Comparison of vehicle velocity and calibrated velocity.

Field Test and Evaluation

A Samsung Galaxy S7 Edge with the Android 5 operating system was used to evaluate the proposed methodology. The GPS was collected at 1 Hz. Gyroscope and accelerometer were at 20 Hz. A total of 100 miles of two-lane highway located on Brookings County and Kingsbury County, South Dakota were selected as the test area. This study considered the curve grade greater than 1 degree of curvature (i.e., curve radius smaller than 5,730 ft). A total of 21 horizontal curves covering different radii were included. For each of these curves, roadway inventory data from the South Dakota Department of Transportation (SDDOT) were used to compare with the estimates. These locations are shown in Figure 8.

Speed Assessment

Vehicle speed plays an important role in this system. To evaluate the speed accuracy, an On-Board Diagnostics (OBD-II) sensor was used to record the velocity from vehicle the speedometer as a reference. Figure 9 illustrates the profile of the calibrated (i.e., GPS) velocity V_t and the reference (i.e., speedometer) velocity V_r from OBD-II sensor.

As shown in Figure 9, the absolute difference between the two speed values is 0–4.5 mph with a mean value of 3.24 mph. The mean absolute percentage error (MAPE) in Equation 14 was used to evaluate the speed deviation:

$$\text{MAPE} = \frac{1}{N}\sum_{n=1}^{N}\left|\frac{V_r - V_t}{V_r}\right| \tag{14}$$

where N is the number of samples.

The MAPE results indicated that there was approximately 6% difference between the GPS and vehicle speeds. This finding is consistent with SenSpeed *(30)*, which utilizes smartphone sensors to sense driving conditions and employs the accelerometer sensor in the smartphone to achieve an average speed error of 2.12 km/h (1.32 mph). Given that the vehicle speedometer is not perfectly accurate, this suggests that the speed precision obtained from the smartphone is acceptable.

Table 1. Radius Measurement without Lane Width Adjustment

No.	Highway and mileage reference marker	Design		Survey 1		Survey 2		Survey 3		Mean	
		G (%)	R (ft)	R	Error	R	Error	R	Error	Average	Error
1	US13@125	5.5	1042	1180	13.24%	1001	3.91%	1040	0.19%	1073	3.05%
2	US13@120	5	1146	1184	3.34%	1166	1.76%	1203	4.94%	1184	3.35%
3	US13@113.28	1.5	3820	3601	5.73%	3676	3.75%	3582	6.21%	3620	5.23%
4	US14@435	2.75	2083	2072	0.55%	2050	1.61%	2083	0.03%	2068	0.73%
5	US14@438	2.5	2292	2296	0.18%	2306	0.61%	2291	0.02%	2298	0.26%
6	US14@402	3	1910	1900	0.51%	1943	1.72%	1866	2.28%	1903	0.36%
7	US14@400.75	11.25	509	455	10.67%	541	6.19%	544	6.87%	513	0.80%
8	US14@397	2.5	2292	2263	1.26%	2268	1.03%	2280	0.49%	2271	0.93%
9	US14@397	2.5	2292	2281	0.48%	2391	4.34%	2287	0.20%	2320	1.22%
10	US14@386	2.75	2083	2083	0.02%	2096	0.60%	2105	1.06%	2095	0.55%
11	US14@385	2.75	2083	2078	0.27%	2046	1.79%	2005	3.75%	2043	1.94%
12	US14@382	2.75	2083	2073	0.50%	2036	2.25%	1956	6.13%	2022	2.96%
13	US14@381.69	2.75	2083	1963	5.80%	1902	8.71%	1972	5.36%	1945	6.62%
14	US14@379.08	2.75	2083	2108	1.20%	2155	3.45%	2058	1.22%	2107	1.14%
15	US14@378.71	10	573	557	2.86%	594	3.65%	550	3.93%	567	1.05%
16	US14B@421.41	3	1910	1895	0.77%	1961	2.66%	1876	1.77%	1911	0.04%
17	US14E@417.08	3	1910	1904	0.33%	1947	1.95%	1909	0.07%	1920	0.52%
18	US30@364.02	4	1432	1495	4.40%	1438	0.40%	1493	4.25%	1476	3.02%
19	US30@365	5	1146	1188	3.71%	1247	8.80%	1214	5.90%	1216	6.14%
20	US30@370	2	2865	2928	2.22%	2961	3.36%	2549	11.03%	2813	1.82%
21	US30@370	2	2865	2663	7.03%	2589	9.62%	2950	2.97%	2734	4.56%
Average difference				3.10%		3.44%		3.27%		2.20%	

Table 2. Radius Measurement with Lane Width Adjustment

No.	Highway and mileage reference marker	Design		Survey 1		Survey 2		Survey 3		Mean	
		G (%)	R (ft)	R	Error	R	Error	R	Error	Average	Error
1	US13@125	5.5	1042	1173	12.57%	1008	3.24%	1033	0.86%	1071	2.82%
2	US13@120	5	1146	1177	2.73%	1159	1.15%	1196	4.33%	1177	2.74%
3	US13@113.28	1.5	3820	3594	5.92%	3683	3.57%	3589	6.03%	3622	5.17%
4	US14@435	2.75	2083	2078	0.26%	2056	1.32%	2089	0.26%	2074	0.44%
5	US14@438	2.5	2292	2290	0.08%	2300	0.35%	2297	0.24%	2296	0.17%
6	US14@402	3	1910	1906	0.20%	1937	1.41%	1872	1.96%	1905	0.25%
7	US14@400.75	11.25	509	461	9.49%	535	5.01%	538	5.69%	511	0.41%
8	US14@397	2.5	2292	2256	1.56%	2275	0.73%	2273	0.80%	2268	1.03%
9	US14@397	2.5	2292	2288	0.17%	2384	4.03%	2294	0.11%	2322	1.32%
10	US14@386	2.75	2083	2091	0.34%	2088	0.24%	2098	0.70%	2092	0.43%
11	US14@385	2.75	2083	2085	0.09%	2054	1.43%	2013	3.39%	2051	1.58%
12	US14@382	2.75	2083	2080	0.14%	2029	2.61%	1963	5.77%	2024	2.84%
13	US14@381.69	2.75	2083	1970	5.44%	1910	8.35%	1979	5.00%	1953	6.26%
14	US14@379.08	2.75	2083	2116	1.56%	2148	3.09%	2065	0.86%	2110	1.26%
15	US14@378.71	10	573	564	1.55%	586	2.34%	558	2.62%	569	0.61%
16	US14B@421.41	3	1910	1901	0.45%	1955	2.34%	1882	1.46%	1913	0.14%
17	US14E@417.08	3	1910	1898	0.64%	1953	2.26%	1915	0.25%	1922	0.62%
18	US30@364.02	4	1432	1489	3.99%	1432	0.02%	1487	3.83%	1470	2.60%
19	US30@365	5	1146	1195	4.28%	1240	8.23%	1220	6.47%	1218	6.33%
20	US30@370	2	2865	2935	2.45%	2954	3.13%	2555	10.81%	2815	1.74%
21	US30@370	2	2865	2670	6.80%	2596	9.39%	2943	2.75%	2736	4.48%
Average difference				2.89%		3.06%		3.06%		2.06%	

Table 3. Superelevation Evaluation

		Survey 1			Survey 2			Survey 3			Mean	
No.	Design elevation (%)	R	Elevation 1 (%)	Error	R	Elevation 2 (%)	Error	R	Elevation 3 (%)	Error	Average	Error
1	5.8	1173	4.0	1.8	1008	7.3	−1.5	1033	5.7	0.1	5.7	0.1
2	5.8	1177	6.8	−1.0	1159	6.2	−0.4	1196	4.1	1.7	5.7	0.1
3	4.6	3594	3.8	0.8	3683	3.0	1.6	3589	5.5	−0.9	4.1	0.5
4	5.6	2078	3.6	2.0	2056	3.2	2.4	2089	7.1	−1.5	4.6	1.0
5	6	2290	6.8	−0.8	2300	7.1	−1.1	2297	3.9	2.1	5.9	0.1
6	5.8	1906	3.8	2.0	1937	7.0	−1.2	1872	3.2	2.6	4.7	1.1
7	4	461	4.5	−0.5	535	5.0	−1.0	538	5.8	−1.8	5.1	−1.1
8	5.8	2256	5.8	0.0	2275	2.9	2.9	2273	6.2	−0.4	4.9	0.9
9	5.8	2288	3.9	1.9	2384	7.4	−1.6	2294	3.7	2.1	5.0	0.8
10	6	2091	3.3	2.7	2088	8.5	−2.5	2098	2.7	3.3	4.8	1.2
11	6	2085	6.8	−0.8	2054	2.4	3.6	2013	7.9	−1.9	5.7	0.3
12	6	2080	3.8	2.2	2029	8.5	−2.5	1963	4.4	1.6	5.6	0.4
13	6	1970	7.8	−1.8	1910	3.5	2.5	1979	8.0	−2.0	6.4	−0.4
14	5.8	2116	3.6	2.2	2148	8.0	−2.2	2065	3.3	2.5	5.0	0.8
15	2.6	564	4.8	−2.2	586	2.0	0.6	558	5.3	−2.7	4.0	−1.4
16	5.6	1901	5.0	0.6	1955	6.2	−0.6	1882	5.1	0.5	5.4	0.2
17	4	1898	4.2	−0.2	1953	3.2	0.8	1915	4.2	−0.2	3.9	0.1
18	5.8	1489	7.0	−1.2	1432	5.3	0.5	1487	7.3	−1.5	6.5	−0.7
19	6	1195	6.6	−0.6	1240	7.5	−1.5	1220	6.9	−0.9	7.0	−1.0
20	4	2935	1.8	2.2	2954	2.6	1.4	2555	5.2	−1.2	3.2	0.8
21	4	2670	3.7	0.3	2596	3.7	0.3	2943	2.0	2.0	3.1	0.9
Average difference			1.32			1.56			1.59		0.66	

Curve Identification and Calculation

Three runs of each survey were measured to evaluate the stability of the proposed approach. All 21 horizontal curves were identified. Table 1 shows the radius measurements without adjusting for the lane width. The results indicated that the average radius difference of three runs is 3.10%, 3.44%, and 3.27%, respectively. The mean radius difference is 2.2%. Table 2 shows the radius with the adjustment of the lane width. The average radius difference of three runs is 2.89%, 3.06%, and 3.06%, respectively. The average error is 2.06%.

The results indicated that drivers might reduce speed when the vehicle is approaching a curve, which generates increased sensor noise, while the sensor data have less noise when leaving the curve because of the reduced speed and smoother driving. This is consistent with previous research findings (*31–33*). For typical superelevation transitions, 90% of the transition occurs before the PC and after the PT. Thus, the majority of the lengths of horizontal curves have full superelevation. Figure 10 shows one case of a superelevation profile measurement with a smartphone. The design superelevation is 4%, while the measured superelevation is 4.2%. Analysis of data from all of the curves indicated that estimating the average of superelevation using data between the 15th and 90th percentile of the length of the curve results in values that are consistent with the design superelevation from the SDDOT roadway inventory.

Table 3 shows the superelevation measurements for the 21 curves. In three runs, the average difference between design superelevation and measured superelevation is 1.32%, 1.56%, and 1.59%, respectively. The overall superelevation difference (i.e., using the average of the three values) is 0.66%. It should be noted that the comparison is between the smartphone-measured superelevation and design superelevation (which may be slightly different from the as-built superelevation). However, as-built superelevation information was not available. Thus, an inclinometer was used to measure the superelevation values for each curve. Natural variation means the measured values changed depending on the specific location that the inclinometer was placed. Using multiple inclinometer measurements at each curve, the superelevation was within 1% of the design superelevation for each of the measurements. Thus, the results in Table 3 are within a reasonable range, particularly when using the mean value of multiple runs.

Conclusions and Discussion

This study presented the design, implementation, and evaluation of a mobile system for low-cost collection of a horizontal curve inventory using a standard smartphone. Although the GPS frequency from smartphones is only 1 Hz, the field test demonstrated that the proposed approach can achieve desirable radius measurement accuracy for sharp curves. The

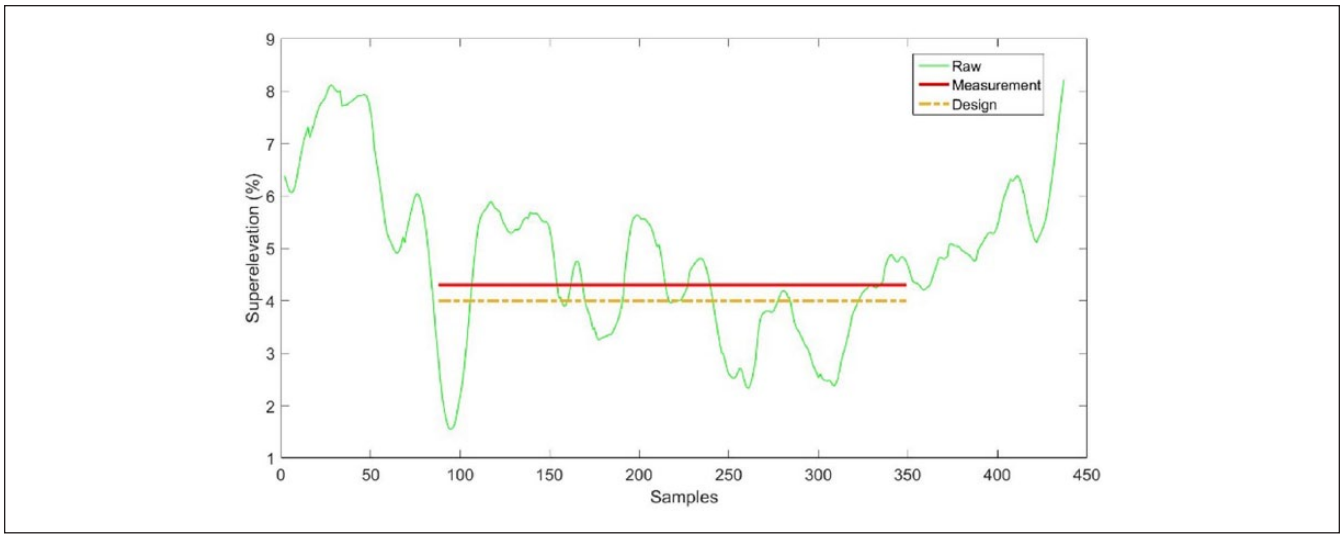

Figure 10. Comparison of design superelevation and measured superelevation.

average error is around 3%. Since the highest accuracy of GPS is 2–5 m, adjusting for differences in lane width does not significantly affect the accuracy of radii estimation. However, multiple runs can achieve higher accuracy. The accuracy of superelevation estimates relies on the accuracy of curve radius, vehicle speed, and acceleration from the smartphone. Improving their accuracy can mean increased accuracy for superelevation estimation.

Off-the-shelf smartphone technology is a potential alternative tool for horizontal curve surveys on account of its low cost and ease of application. However, the EKF approach for correcting GPS is sustainable only over a few seconds when there is a GPS outage. Longer GPS outage will result in larger location error. In addition, this research focused on applying this technology to measuring simple, sharp horizontal curves. Future work should include compound, reverse, and spiral curves using smartphone sensors. The GPS frequency from current smartphones is only 1 Hz. Increasing the frequency of the GPS measurements could potentially improve the radius estimation. GPS/IMU sensor fusion should be considered to increase the frequency of GPS in future work.

References

1. Zeeger, C. *NCHRP Report 362: Roadway Widths for Low-Traffic Volume Roads*. HRB, National Research Council,, Washington, D.C., 1994.
2. National Highway Traffic Safety Administration. *Traffic Safety Facts 2014*. National Highway Traffic Safety Administration, Washington, D.C., 2015, p. 87.
3. Li, Z., M. V. Chitturi, A. R. Bill, D. Zheng, and D. A. Noyce. Automated extraction of horizontal curve information for low-volume roads. *Transportation Research Record: Journal of the Transportation Research Board*, 2015. 2472: 172–184.
4. U.S. Department of Transportation. *Manual on Uniform Traffic Control Devices for Streets and Highways*. U.S. Department of Transportation, Washington, D.C., 2009.
5. Xu, H., and D. Wei. Improved Identification and Calculation of Horizontal Curves with Geographic Information System Road Layers. *Transportation Research Record: Journal of the Transportation Research Board*, 2016. 2595: 50–58.
6. Findley, D. J., C. V. Zegeer, C. A. Sundstrom, J. E. Hummer, W. Rasdorf, and T. J. Fowler. Finding and Measuring Horizontal Curves in a Large Highway Network: a GIS Approach. *Public Works Management & Policy*, Vol. 17, No. 2, 2012, pp. 189–211.
7. Yang, Y., and C. Zhu. Extracting Road Centrelines from High-resolution Satellite Images Using Active Window Line Segment Matching and Improved SSDA. *International Journal of Remote Sensing*, Vol. 31, No. 9, 2010, pp. 2457–2469.
8. Shi, W., Z. Miao, and J. Debayle. An Integrated Method for Urban Main-Road Centerline Extraction from Optical Remotely Sensed Imagery. *IEEE Transactions on Geoscience and Remote Sensing*, Vol. 52, No. 6, 2014, pp. 3359–3372.
9. Miao, Z., B. Wang, W. Shi, and H. Wu. A Method for Accurate Road Centerline Extraction from a Classified Image. *IEEE Journal of Selected Topics in Applied Earth Observations and Remote Sensing*, Vol. 7, No. 12, 2014, pp. 4762–4771.
10. Miao, Z., W. Shi, H. Zhang, and X. Wang. Road Centerline Extraction from High-resolution Imagery Based on Shape Features and Multivariate Adaptive Regression Splines. *IEEE Geoscience and Remote Sensing Letters*, Vol. 10, No. 3, 2013, pp. 583–587.
11. Harkey, D., C. Yi, and J. Feaganes. Evaluation and Validation of Automated In-Vehicle Data Collection System for Developing Roadway Alignments. *Transportation Research Record: Journal of the Transportation Research Board*, 2004. 1897: 164–172.
12. Carlson, P. J., M. B. Kit Black, and E. R. Rose. Comparison of Radius-Estimating Techniques for Horizontal Curves. *Transportation Research Record: Journal of the Transportation Research Board*, 2005. 1918: 76–83.

13. Findley, D. J., J. E. Hummer, W. Rasdorf, and B. T. Laton. Collecting Horizontal Curve Data: Mobile Asset Vehicles and Other Techniques. *Journal of Infrastructure Systems*, Vol. 19, No. 1, 2012, pp. 74–84.
14. Kim, J., J.-C. Lee, I.-J. Kang, S.-Y. Cha, H. Choi, and T.-G. Lee. Extraction of Geometric Information on Highway Using Terrestrial Laser Scanning Technology. *International Archives of the Photogrammetry, Remote Sensing and Spatial Information Sciences*, Vol. 37, 2008, pp. 539–544.
15. Jalayer, M., H. Zhou, J. Gong, S. Hu, and M. Grinter. A Comprehensive Assessment of Highway Inventory Data Collection Methods. *Journal of the Transportation Research Forum*, Vol. 53, 2014, pp. 73–92.
16. Qin, X., S. Zhang, and W. Wang. Avoiding Roadway Departure Crashes with an In-Vehicle Head-Up Display. Presented at the Transportation Research Board 94th Annual Meeting, 2015.
17. Aichinger, C., P. Nitsche, R. Stütz, and M. Harnisch. Using Low-cost Smartphone Sensor Data for Locating Crash Risk Spots in a Road Network. *Transportation Research Procedia*, Vol. 14, 2016, pp. 2015–2024.
18. Lee, S., G. Tewolde, and J. Kwon. Design and Implementation of Vehicle Tracking System Using GPS/GSM/GPRS Technology and Smartphone Application. *IEEE World Forum on Internet of Things (WF-IoT)*, Seoul, South Korea, 2014, pp. 353–358.
19. Ghose, A., P. Biswas, C. Bhaumik, M. Sharma, A. Pal, and A. Jha. Road Condition Monitoring and Alert Application: Using In-Vehicle Smartphone as Internet-Connected Sensor. *2012 IEEE International Conference on Pervasive Computing and Communications Workshops (PERCOM Workshops)*, Lugano, Switzerland, 2012, pp. 489–491.
20. Raj, S., A. Jain, and R. Misra. Smartphone Sensing for Large Data Set Collection of Potholes. *Proc., 11th Annual International Conference on Mobile Systems, Applications, and Services*, Taipei, Taiwan, 2013, pp. 517–518.
21. Islam, S., W. Buttlar, R. Aldunate, and W. Vavrik. Measurement of Pavement Roughness Using Android-based Smartphone Application. *Transportation Research Record: Journal of the Transportation Research Board*, 2014. 2457: 30–38.
22. Buttlar, W. G., and M. S. Islam. *Integration of Smart-Phone-Based Pavement Roughness Data Collection Tool with Asset Management System*. NEXTRANS Project No. 098IY04. University of Illinois at Urbana-Champaign, 2014.
23. Won, M., Z. Shaohu, A. Chekuri, and S. H. Son. Enabling Energy-Efficient Driving Route Detection Using Built-in Smartphone Barometer Sensor. *2016 IEEE 19th International Conference on Intelligent Transportation Systems (ITSC)*, Rio de Janeiro, Brazil, 2016, pp. 2378–2385.
24. Zhang, S., M. Won, and S. H. Son. *Low-Cost Realtime Horizontal Curve Detection Using Inertial Sensors of a Smartphone*. Presented at the 84th IEEE Vehicular Technology Conference, Montréal, Canada, 2016.
25. Guo, H., M. Yu, J. Liu, and J. Ning. Butterworth Low-Pass Filter for Processing Inertial Navigation System Raw Data. *Journal of Surveying Engineering*, Vol. 130, No. 4, 2004, pp. 175–178.
26. Haykin, S. S. *Kalman Filtering and Neural Networks*. Wiley, New York, 2001.
27. Steinley, D. K-means Clustering: A Half-Century Synthesis. *British Journal of Mathematical and Statistical Psychology*, Vol. 59, No. 1, 2006, pp. 1–34.
28. Han, J., J. Pei, and M. Kamber. *Data Mining: Concepts and Techniques*. Elsevier, Amsterdam, 2011.
29. American Association of State Highway and Transportation Officials. *A Policy on Geometric Design of Highways and Streets*, 6th ed. AASHTO, Washington, D.C., 2011.
30. Yu, J., H. Zhu, H. Han, Y. J. Chen, J. Yang, Y. Zhu, Z. Chen, G. Xue, and M. Li. Senspeed: Sensing Driving Conditions to Estimate Vehicle Speed in Urban Environments. *IEEE Transactions on Mobile Computing*, Vol. 15, No. 1, 2016, pp. 202–216.
31. Figueroa Medina, A., and A. Tarko. Speed Factors on Two-lane Rural Highways in Free-Flow Conditions. *Transportation Research Record: Journal of the Transportation Research Board*, 2005. 1912: 39–46.
32. Hu, W., and E. T. Donnell. Models of Acceleration and Deceleration Rates on a Complex Two-Lane Rural Highway: Results from a Nighttime Driving Experiment. *Transportation Research Part F: Traffic Psychology and Behaviour*, Vol. 13, No. 6, 2010, pp. 397–408.
33. Wood, J., and E. Donnell. Stopping Sight Distance and Horizontal Sight Line Offsets at Horizontal Curves. *Transportation Research Record: Journal of the Transportation Research Board*, 2014. 2436: 43–50.

The Standing Committee on Geometric Design peer-reviewed this paper (18-04114).